Neutron to proton ratios of quasiprojectile and midrapidity emission in the ^{58}Ni+^{58}Ni reaction at 52 MeV/nucleon

D. Thériault,[1,*] A. Vallée,[1] L. Gingras,[1] Y. Larochelle,[1] R. Roy,[1] A. April,[1] L. Beaulieu,[1] F. Grenier,[1] F. Lemieux,[1] J. Moisan,[1] M. Samri,[2] C. St-Pierre,[1] S. Turbide,[1,†] B. Borderie,[3] R. Bougault,[4] P. Buchet,[5] J. L. Charvet,[5] A. Chbihi,[6] J. Colin,[4] D. Cussol,[4] R. Dayras,[5] D. Durand,[4] J. D. Frankland,[6] E. Galichet,[3,7] D. Guinet,[8] B. Guiot,[6] P. Lautesse,[8] J. F. Lecolley,[4] N. Le Neindre,[6] O. Lopez,[4] A. M. Maskay,[8] L. Nalpas,[5] M. Parlog,[9] P. Pawlowski,[10] M. F. Rivet,[3] E. Rosato,[11] J. C. Steckmeyer,[4] B. Tamain,[4] E. Vient,[4] C. Volant,[5] J. P. Wieleczko,[6] INDRA Collaboration, S. J. Yennello,[12] E. Martin,[12] and E. Winchester[12]

[1]*Laboratoire de Physique Nucléaire, Département de Physique, Université Laval, Québec, Canada G1K 7P4*

[2]*Laboratoire de Physique Nucléaire et Applications, Université Ibn Tofail, Kénitra, Morocco*

[3]*Institut de Physique Nucléaire, IN2P3-CNRS, F-91406 Orsay Cedex, France*

[4]*LPC, IN2P3-CNRS, ISMRA and Université, F-14050 Caen Cedex, France*

[5]*DAPNIA/SPhN, CEA/Saclay, F-91191 Gif sur Yvette Cedex, France*

[6]*GANIL, CEA and IN2P3-CNRS, B.P. 5027, F-14076 Caen Cedex, France*

[7]*Conservatoire National des Arts et Métiers, F-75141 Paris Cedex 03, France*

[8]*Institut de Physique Nucléaire, IN2P3-CNRS and Université, F-69622 Villeurbanne Cedex, France*

[9]*National Institute for Physics and Nuclear Engineering, RO-76900 Bucharest-Magurele, Romania*

[10]*H. Niewodniczanski Institute of Physics, Radzikowskiego 152, 31-342 Kraków, Poland*

[11]*Dipartimento di Scienze Fisiche and Sezione INFN, Università di Napoli "Federico II", I-80126 Napoli, Italy*

[12]*Cyclotron Institute, Texas A&M University, College Station, Texas*

(Received 2 March 2004; published 27 January 2005)

By combining data from a charged particle ^{58} Ni+^{58}Ni experiment at 52 MeV/nucleon with an ^{36}Ar+^{58}Ni experiment at 50 MeV/nucleon for which free neutrons have been detected, an increase in the neutron to proton ratio of the whole nuclear material at midrapidity has been experimentally observed in the reaction ^{58}Ni+^{58}Ni at 52 MeV/nucleon. The neutron-to-proton ratio of the quasi-projectile emission is analyzed for the same reactions and is seen to decrease below the ratio of the initial system. Those observations suggest that an asymmetric exchange of neutrons and protons between the quasiprojectile and the midrapidity region exists.

DOI: 10.1103/PhysRevC.71.014610 PACS number(s): 25.70.Lm, 25.70.Mn

I. INTRODUCTION

In recent years, a source of emission between the target rapidity and that of the projectile has been evidenced and characterized in heavy ions collisions at intermediate energies [1–14] and theoretically studied [15,16]. Interestingly, light particles and fragments emitted by that midrapidity source (MRS) exhibit a neutron enrichment compared to those from the quasiprojectile (QP) or the quasitarget (QT) [17–20]. This fact could be due to the abundance of symmetric clusters [21] or Coulomb effects [21,22] and does not necessarily imply a neutron enrichment of the total nuclear matter at midrapidity. Therefore, the analysis of the whole MRS material is of interest. To explain the neutron abundance of a supposed low-density MRS, a density dependence in the symmetry energy term of the nuclear equation of state has been suggested [23–26]. Experimental results with free-neutron detection have been obtained in the reaction ^{129}Xe+^{nat}Sn at 40 MeV/nucleon [21]. The conclusions of the authors were that, on average (for semiperipheral collisions), the MRS and the bulk system have an indistinguishable value of their N/Z ratios. In the present article, we report on an experimental evaluation of the MRS and QP N/Z ratios as a function of the centrality of the collision. A smaller system with a lower N/Z ratio than in [21], the ^{58}Ni+^{58}Ni reaction, is studied at 52 MeV/nucleon and the free-neutron multiplicities are extracted from the analysis of the ^{36}Ar+^{58}Ni reaction at 50 MeV/nucleon. Experimental setups are first described. Methods of the QP reconstruction and the MRS selection are then presented. This is followed by moving source analyses for protons in ^{58}Ni+^{58}Ni and for neutrons from the ^{36}Ar+^{58}Ni reaction. Evaluation of the N/Z ratios for the MRS and QP in ^{58}Ni+^{58}Ni follows. Finally, discussion about the results and a proposed picture of the phenomena leading to them are presented.

II. EXPERIMENTAL APPARATUS

A. INDRA experiment

The charged particle experiment has been performed at the GANIL facility using a ^{58}Ni beam accelerated to 52 MeV/nucleon bombarding a self-supporting 0.179 mg/cm^2 ^{58}Ni target. The charged reaction products were detected with the INDRA detector, which consists of 336 detection modules mounted on 17 rings covering polar angles from 2° to 176°. The first inner ring is made of fast-slow plastic phoswich detectors. Rings 2–9 consist of a triple telescope, with an

*Correspondence to D. Thériault, email: dtheriau@phy.ulaval.ca.

†Present address: McGill University, Montréal, Québec,Canada.

ionization chamber, SI detector, and CsI(Tl) scintillator. Rings 10–17 consist of an ionization chamber and a CsI scintillator. Elements were identified by their charge up to $Z = 28$ in the forward region and isotopic resolution was achieved up to $Z = 4$. The electronic trigger required a multiplicity of 4 detection modules to fire in the array. A complete description of the INDRA detector is given in Ref. [27].

B. HERACLES experiment

For the neutron detection experiment at the Cyclotron Institute of Texas A&M University, a ^{36}Ar beam has been accelerated to 50 MeV/nucleon on a 5.0 mg/cm^2 ^{58}Ni target. The charged reaction products were collected with the HERACLES multidetector array. The first five rings of the array are made of fast-slow plastic phoswich detectors located between 1.3° and 24°. Those detectors have energy detection thresholds of 7.5 (27.5) MeV/nucleon for element identification of $Z = 1$ (28) particles. Two other rings, covering angles from 24° to 46°, are made of CsI(Tl) scintillators providing charge and isotopic resolution for $Z = 1$,2 and 3 elements with an energy threshold of about 2 MeV/nucleon. The electronic trigger required a multiplicity of three fired detectors in the charged particle array. Neutrons were detected with Bicron BC-501 liquid scintillator units located outside the reaction chamber at polar angles of 60°, 75°, 90°, 120°, 135°, and 150°. Neutron energies were determined by time-of-flight measurements and spectra were corrected for background emission using a shadow bar technique. The fraction of background neutrons was around 30%. An experimental response function for the BC-501 detector [28] was used to correct the spectra for detection efficiency. For neutron energy below 5 MeV, efficiency is computed with the SCINFUL code [28]. Attenuation in the chamber wall was taken into account. Thresholds of neutron identification were between 100 and 600 keVee.

III. ANALYSIS

A. Source and event selection in ^{58}Ni+^{58}Ni

In the present analysis, only isotopically well identified elements ranging from $Z = 1$ to $Z = 4$ were used in rings 2–12 of the INDRA multidetector (3°–88°). Events containing nonisotopically resolved elements from $Z = 1$ to $Z = 4$ in those forward rings were rejected. The elements with $Z \geqslant 5$ were accepted in rings 1–9 of the INDRA multidetector (2° to 45°). The mass assumed for those heavier elements is based on the evaporation attractor line of Charity [29] or on the initial N/Z of the system for $Z \geqslant 25$. The MRS is not affected by those last analysis conditions, because it is composed almost exclusively of $Z = 1$–4 elements. It was verified that $Z \geqslant 5$ fragments above 45° would negligibly contribute to the MRS and are not significant in the present analysis. The heaviest fragment in the forward direction is taken as the QP evaporation residue. Events selection criteria are as follows: parallel velocity of the residue greater than 70% of the beam velocity and charge of the residue (Z_{res})

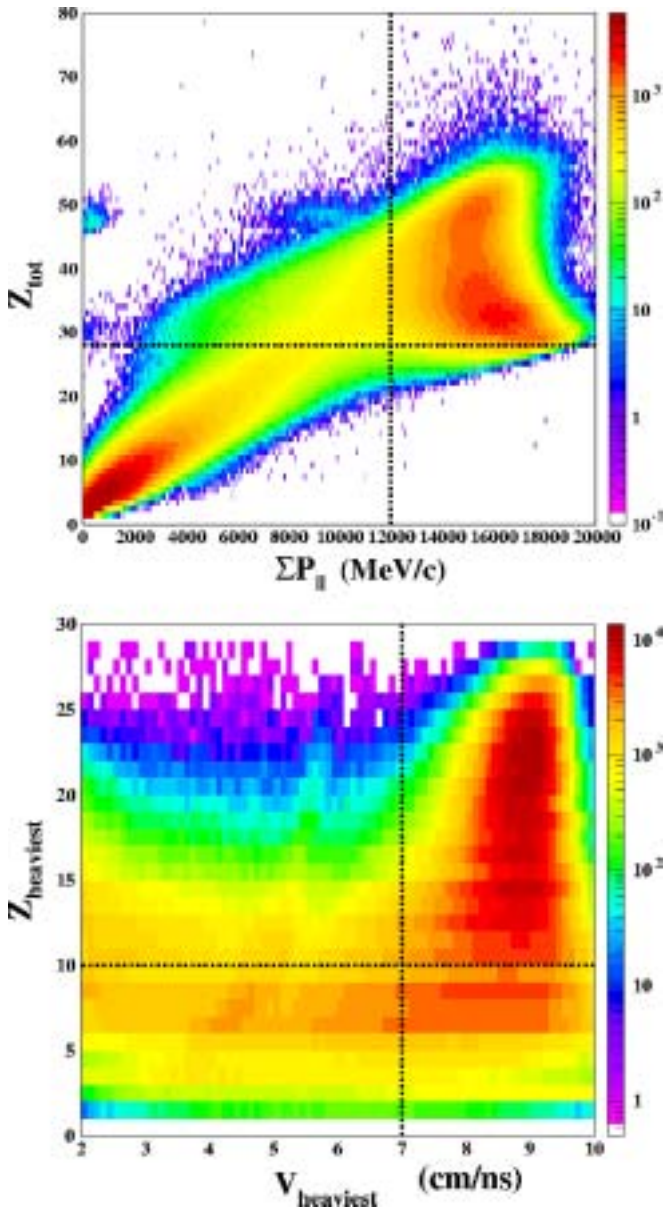

FIG. 1. (Color online) Total detected charge vs. total detected parallel (beam direction) momentum (upper panel) and charge of the heaviest fragment vs. parallel velocity of the heaviest fragment (lower panel). Graphics are for the ^{58}Ni+^{58}Ni reaction at 52 MeV/nucleon and limits for the sample of events analyzed are indicated with dashed lines.

greater or equal to 10. This selection of peripheral and midperipheral events is made to avoid contamination of the QP forward hemisphere (particles with parallel velocities greater than that of the residue) by other sources or nonstatistical emission and to apply the QP reconstruction procedure in its optimal range of efficiency. However, the electronic trigger requirement (multiplicity of four detection modules fired) and the reaction grazing angle below the first ring of the INDRA detector prohibit the detection of the most peripheral reactions. Although the term *peripheral* is used, selected events present a certain degree of dissipation and exclude the most peripheral reactions. Also, only events with a total detected charge of 28

or more in the INDRA multidetector and $\Sigma P_{\parallel} \geqslant 66\% P_{\parallel \text{initial}}$ were analyzed, $\Sigma P_{\parallel}$ being the beam direction momentum component of all particles. Figure 1 illustrates the event selection. Selected events represent a cross section of about 160 mb.

Because the goal of the present analysis is to evaluate the MRS and QP N/Z ratios as a function of centrality in the ^{58}Ni+^{58}Ni reaction at 52 MeV/nucleon, it is important to disentangle the QP emitted material from the nuclear material emitted by the MRS in this reaction. Attribution of bound particles ($A \geqslant 2$) to the QP source is done via a weighting method. MRS emission is selected as non-QP particles with a parallel (beam direction) velocity higher than a specified velocity cut to isolate them from QT emission. The free protons and neutrons, because of a significant overlap in source emission, were treated differently. Multisource analysis for free nucleons is presented in Secs. III C and III D.

B. Cluster attribution in ^{58}Ni+^{58}Ni

The QP source reconstruction procedure, applied to the ^{58}Ni+^{58}Ni reaction, relies on three hypotheses [30]: (a) the heaviest fragment selected as the QP evaporation residue has a velocity that is a approximatively the QP velocity, (b) the QP emission is isotropic in its reference frame, and (c) all the particles with a parallel velocity greater than that of the residue (forward distribution) were emitted from the QP. V_{rel} (norm of the relative velocity between a particle and the residue) spectra are made for each pair of isotope and charge of residue (Z_{res}). Using V_{rel} spectra, probability tables for the attribution of an isotope to the QP are built. Attribution probability is fixed at unity for forward emitted particles, whereas the probability for backward particles (parallel velocity less than that of the QP residue) is obtained by dividing the forward V_{rel} distribution by the backward distribution. The probability tables are applied on an event-by-event basis to reconstruct the QP, each particle in the backward distribution having a probability to be attributed to the QP according to its specific value of V_{rel} and Z_{res}. Figure 2 shows examples of V_{rel} spectra for He and Li isotopes with $Z_{\text{res}} = 15$ and $Z_{\text{res}} = 14$, respectively. The QP reconstruction procedure applied to DIT+GEMINI [31,32] simulated events has been shown to give more than 85% of good attribution for particles emitted in midperipheral and peripheral collisions of the reaction ^{58}Ni+^{12}C at 34.5 MeV/nucleon [30]. More details about the reconstruction method and its efficiency are given in Refs. [7,9,10,30].

Backward emitted particles that were not attributed to the QP were attributed to the MRS if their parallel velocity was greater than 2 cm/ns in the reference frame of the QT, which is moving at velocities determined in the proton multisource analysis (see Table I). That limit, 2 cm/ns, is a confidence value established from the QP parallel velocity distributions in the forward distribution to build a MRS sample with little pollution from the QT. Graphs used to establish this velocity cut are similar to those of Fig. 2 projected over the parallel direction only. Figure 3 shows the mean number of protons and neutrons in bound particles and fragments emitted from the QP and MRS, excluding free nucleons and the QP residue.

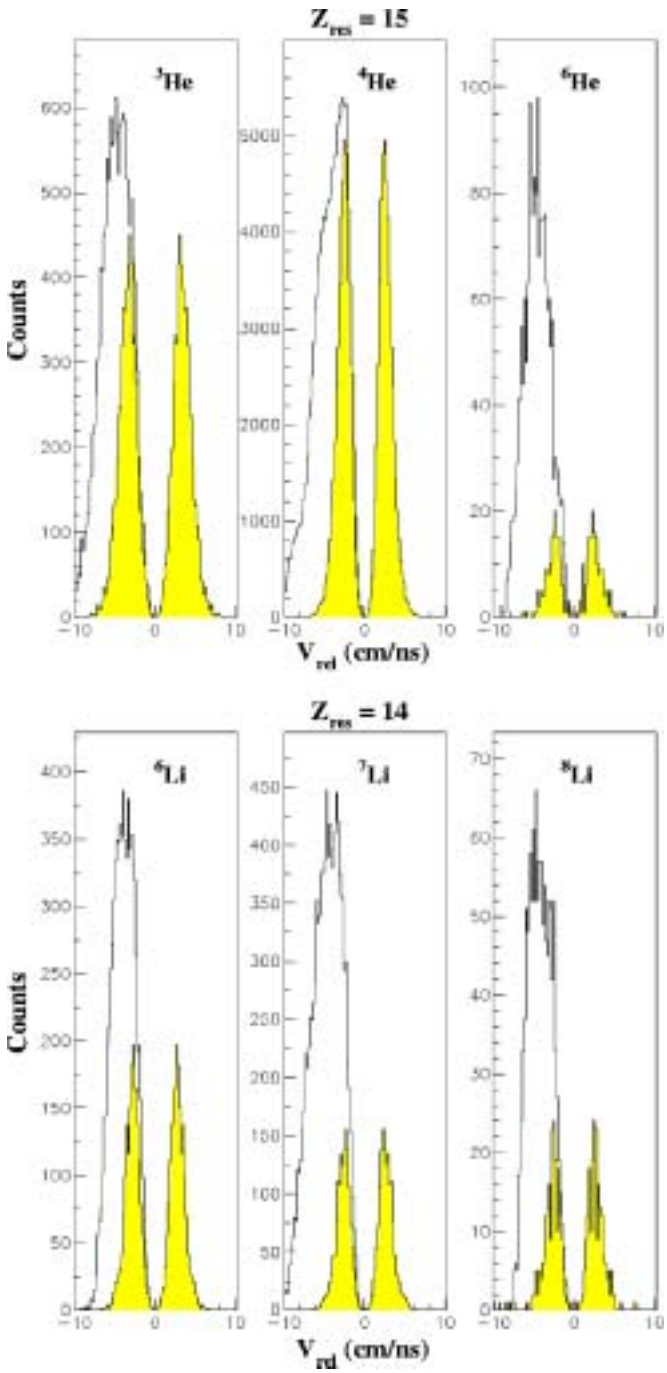

FIG. 2. (Color online) Total V_{rel} distribution (clear) and positive V_{rel} distribution backward-reflected (shadowed) for $Z = 2$ isotopes coupled with a QP residue of $Z = 15$ (upper panel) and for $Z = 3$ isotopes coupled with a QP residue of $Z = 14$ (lower panel). V_{rel} (norm of the relative velocity with the residue) distributions are from the reaction ^{58}Ni+^{58}Ni at 52 MeV/nucleon.

The number of bound nucleons as a function of the charge of the projectile minus the charge of the QP residue ($Z_{\text{proj}} - Z_{\text{res}}$), exhibit a clear difference between MRS and QP emission. The quantity $Z_{\text{proj}} - Z_{\text{res}}$ will be shown to be proportional to the QP excitation energy per nucleon and thus to the centrality of the collision [13]. An increase of MRS bound neutrons,

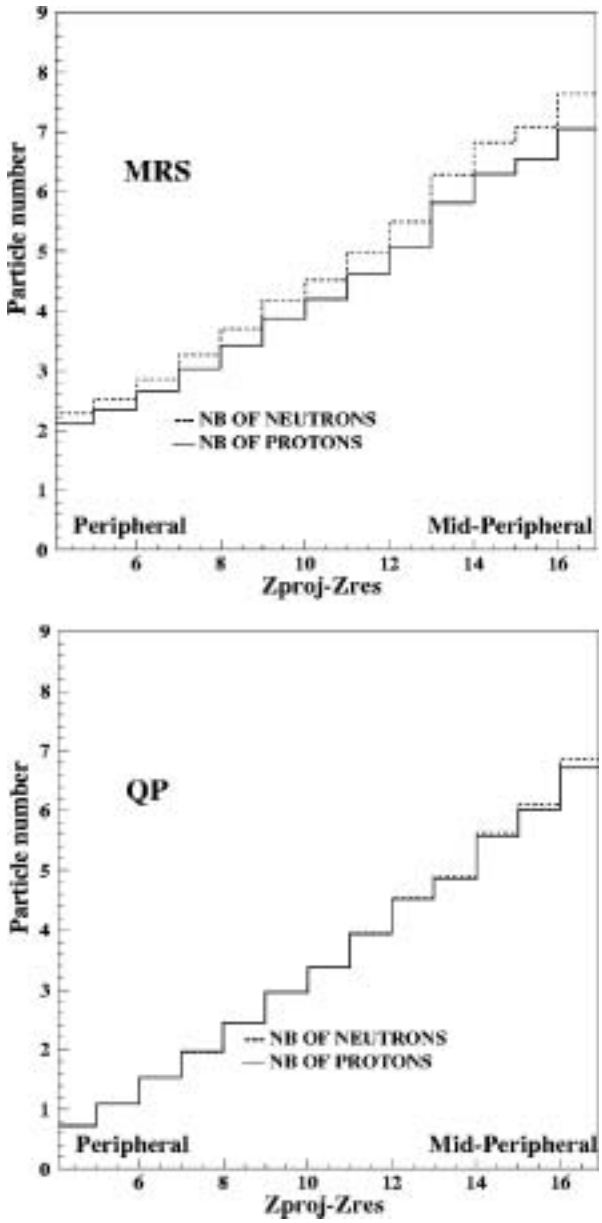

FIG. 3. Number of neutrons (dashed lines) and protons (full lines) in $A \geqslant 2$ bound particles and fragments for MRS (upper panel) and QP (lower panel) for the reaction ^{58}Ni+^{58}Ni at 52 MeV/nucleon. The graphics exclude free nucleons and QP residue. Statistical error for $Z_{\text{proj}} - Z_{\text{res}} = 14$ is equal to 0.02.

compared to bound protons, is seen as a function of the centrality, whereas for the QP, the emission is rather symmetric regarding protons and neutrons over the whole collision range. These results agree with the abundance of neutron-rich IMFs (intermediate mass fragments) and particles observed at midrapidity [17–20]. Figure 3 also displays the importance of midrapidity and QP emission as a function of centrality, showing the number of neutrons and the number of protons emitted by those two process as a function of the centrality parameter.

C. Free proton evaluation in ^{58}Ni+^{58}Ni

To include free protons in the analysis, average proton multiplicities are extracted for four classes of events sorted according to $Z_{\text{res}}(^{58}\text{Ni})$: 10–13, 14–18, 19–23, and 24–28, characterizing the centrality of the reaction. Multiplicities are obtained via moving source analysis of energy spectra at 16 angles from the INDRA detector. The energy spectra are fitted simultaneously with the summation of three sources, QP, QT, and MRS, each being characterized by its temperature T, its velocity V_s, its Coulomb barrier B_c, and its proton multiplicity N. The proton energy (E) distribution is fitted under the assumption of surface emission for the QT and QP sources and volume emission for the MRS by [13,33–37]:

$$\left(\frac{d^2\sigma}{d\Omega dE}\right)_{\text{sur}} = \frac{N}{4\pi T^2}(E - B_c)\exp[-(E - B_c)/T] \quad (1)$$

and

$$\left(\frac{d^2\sigma}{d\Omega dE}\right)_{\text{vol}} = \frac{N}{2(\pi T)^{3/2}}\sqrt{(E - B_c)}\exp[-(E - B_c)/T] \quad (2)$$

respectively. The transformation to the laboratory frame takes into account the angle θ of the detector and the velocity V_S of the emitting source according to the equation

$$\left(\frac{d^2\sigma}{d\Omega dE}\right)_{\text{lab}} = \left(\frac{E_{\text{lab}}}{E'}\right)^{1/2}\left(\frac{d^2\sigma}{d\Omega dE}\right)_{E=E'} \quad (3)$$

where

$$E' = E_{\text{lab}} - 2{E_{\text{lab}}}^{1/2}E_s^{1/2}\cos\theta + E_s \quad (4)$$

Here, E_s is the kinetic energy of a proton at rest in the source reference frame moving at velocity V_s. Extracted velocity and multiplicity parameters for protons in the reaction ^{58}Ni+^{58}Ni are displayed in Table I for all classes of events. Overall, proton multiplicities increase smoothly with centrality. MRS velocities are always near the nucleon-nucleon velocity (5.02 cm/ns). QP(QT) velocities decrease (increase) with centrality. Coulomb barrier parameter for QP and QT are between 0 and 2 MeV. Figure 4 presents the results of the multisource fit for all the centrality classes at selected angles. Except for kinematic effects in the extreme forward direction due to the model of an emitting sphere with a Coulomb barrier [35], the fit is in good agreement with the data. Figure 5 shows the extracted proton multiplicities as a function of $Z_{\text{proj}}(^{58}\text{Ni}) - Z_{\text{res}}(^{58}\text{Ni})$.

D. Free neutron evaluation in ^{36}Ar+^{58}Ni

The multisource fit for free neutrons is done on spectra from the ^{36}Ar+^{58}Ni experiment. The events are sorted into four classes according to $Z_{\text{res}}(^{36}\text{Ar})$: 4–6, 7–9, 10–14, and 15–20. Because forward angles were not covered by the neutron detectors, energy spectra are fitted with the summation of two moving sources, QT and MRS. A third source of emission (QP) has also been tried but its contribution was found negligible at 60° and above. The neutron energy distribution is fitted under the assumption of surface emission for the QT source

TABLE I. (a) Source velocities (V_s, cm/ns) and mean neutron multiplicities (N) for the QT and MRS in ^{36}Ar+^{58}Ni reaction at 50 MeV/nucleon. (b) Source velocities (V_s, cm/ns) for the QT, QP and MRS and mean proton multiplicities (N) for the QP and MRS in ^{58}Ni+^{58}Ni reaction at 52 MeV/nucleon.

(a) ^{36}Ar+^{58}Ni 50 MeV/nucleon	HERACLES			
	QT(Ni)		MRS	
Centrality	V_s(cm/ns)	N(n.)	V_s(cm/ns)	N(n.)
$4 \leqslant Z_{res_{Ar}} \leqslant 6$	1.10	1.08	4.98	2.30
$7 \leqslant Z_{res_{Ar}} \leqslant 9$	0.97	1.24	5.10	1.67
$10 \leqslant Z_{res_{Ar}} \leqslant 14$	0.53	0.67	2.11	0.69
$15 \leqslant Z_{res_{Ar}} \leqslant 20$	0.54	0.71	2.11	0.18
(b) ^{58}Ni+^{58}Ni 52 MeV/nucleon	INDRA			
	QT(Ni)		MRS		QP(Ni)	
Centrality	V_s		V_s(cm/ns)	N(p.)	V_s(cm/ns)	N(p.)
$10 \leqslant Z_{res} \leqslant 13$	1.16		4.54	1.77	8.98	2.96
$14 \leqslant Z_{res} \leqslant 18$	0.80		5.10	1.76	9.56	2.36
$19 \leqslant Z_{res} \leqslant 23$	0.27		5.13	1.06	9.58	2.57
$24 \leqslant Z_{res} \leqslant 28$	0.00		4.09	0.99	9.63	2.09

and volume emission for the MRS, using Eqs. (1) and (2) without Coulomb barriers. All six neutron spectra of a given centrality class are fitted simultaneously [34]. Figure 6 shows fits of the neutron energy spectra for the different classes. Figure 7 presents the corresponding free neutron multiplicities as a function of the projectile charge minus the QP residue charge. Extracted velocity parameters and multiplicities for neutrons are displayed in Table I for all classes of events.

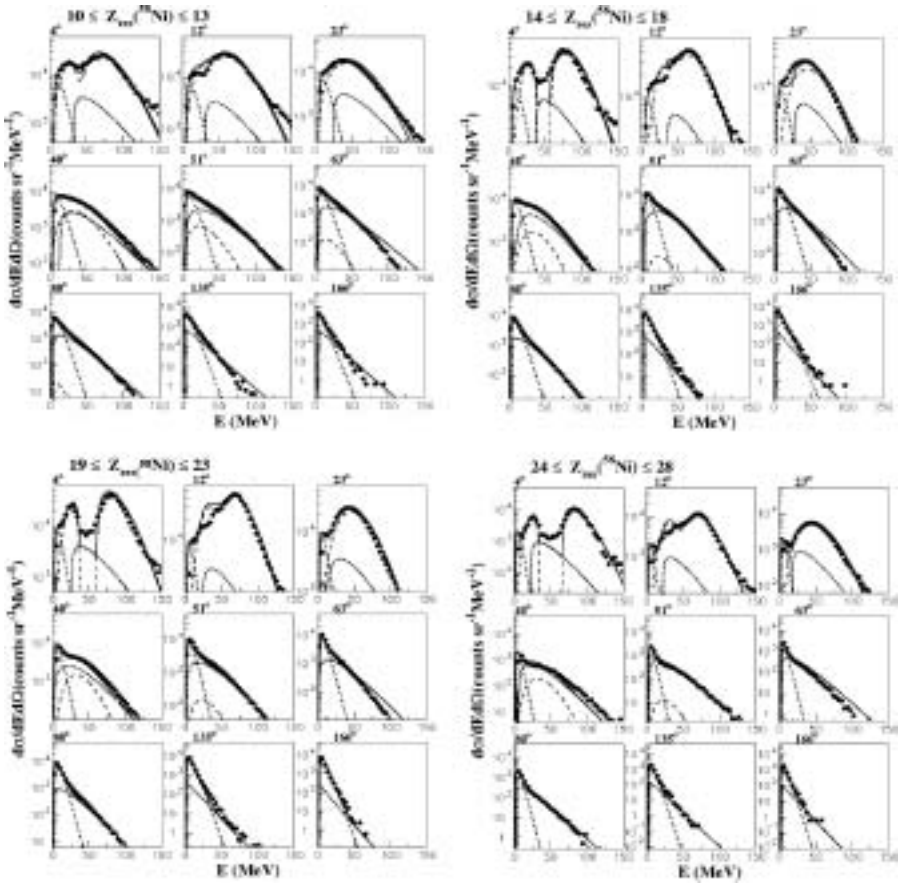

FIG. 4. Multisource fit for free protons at selected angles for the reaction ^{58}Ni+^{58}Ni at 52 MeV/nucleon. The four centrality classes defined with the charge of the QP residue are shown. QP (dashed lines), QT (dotted lines), MRS (dotted-dashed lines), and total (full lines) contributions are illustrated.

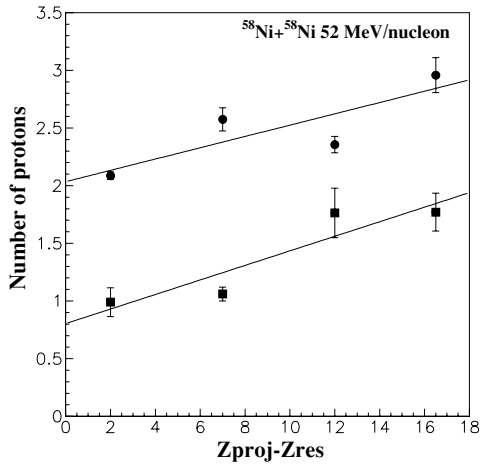

FIG. 5. Linearized proton multiplicities for ^{58}Ni+^{58}Ni at 52 MeV/nucleon as a function of the projectile charge minus the QP residue charge. QP (dots) and MRS (squares) multiplicities are illustrated. For each class of reaction, extracted multiplicities were placed at the center of their $Z_{\rm res}$ interval.

The MRS velocity in ^{36}Ar+^{58}Ni increases from peripheral to central collisions. The velocity goes from a value of 2.1 cm/ns in the two most peripheral collision classes to a near nucleon-nucleon velocity (4.9 cm/ns) for the most central ones. This tendency for MRS source velocities extracted with free neutrons can be interpreted in the framework of recent findings on MRS emission [7,8,16]. According to those previous results, MRS emission can be regarded as a sum of two kinds of emitting phenomena: prompt emission, which for free nucleons should occur at an average nucleon-nucleon velocity, and a delayed emission that occurs after the rupture of a "neck-type" dynamical deformation between QP and QT. This delayed emission has been shown to take place near the surface of the QP or QT [7,8,16] and to be enhanced on the velocity side of the heaviest partner of the reaction [7,16]. It has been observed in peripheral collisions [8] for IMFs but was also shown to exist for $Z = 2$ particles [7]. The proposed dynamical origin of this emission does not prevent, a priori, this emission to take place for free nucleons. In the present case, extracted MRS velocities could be explained by the fraction of free neutrons emitted by the two mechanisms described above. In peripheral and semiperipheral collisions, free neutrons might come from both mechanisms with a predominance of the "neck-type" dynamical deformation. The lack of Coulomb influence on the free neutrons should make the proximity of the delayed dynamical emission near the QT even more evident. In more central collisions, preequilibrium particles become more abundant due to the increase of the geometrical overlap between the nuclei, which could explain the tendancy toward a near nucleon-nucleon velocity. Tests conducted for

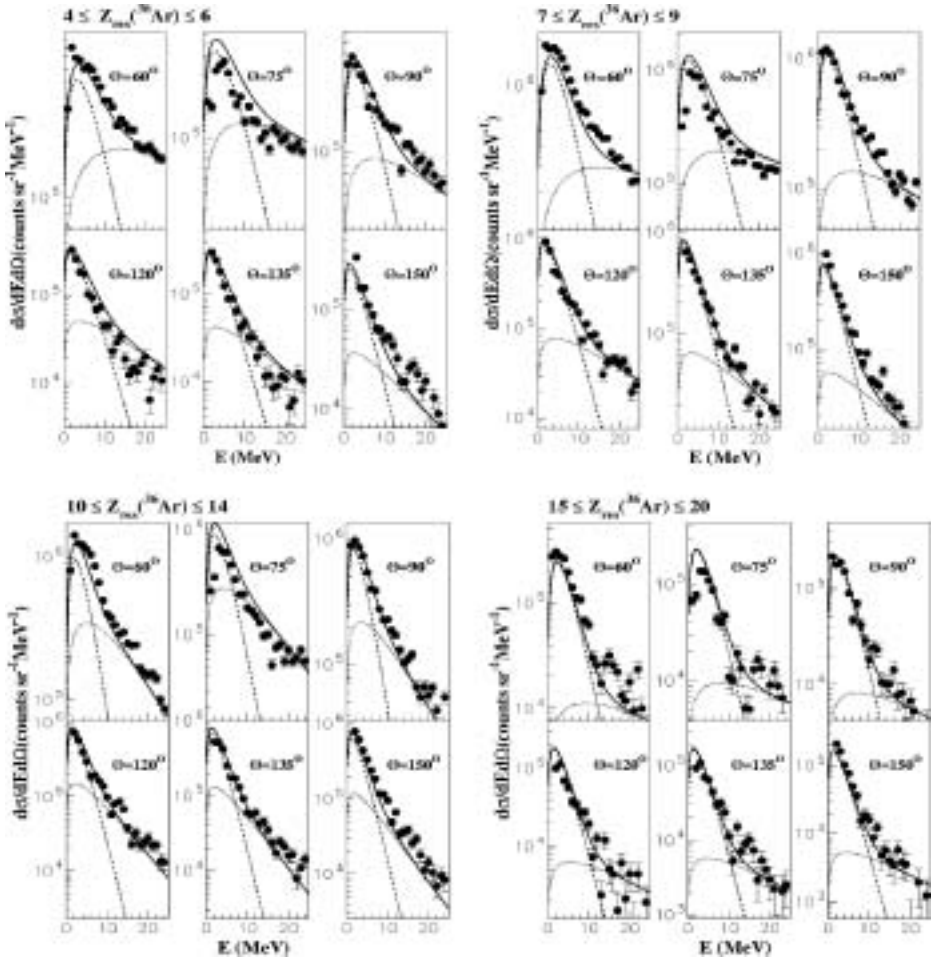

FIG. 6. Neutron energy spectra corrected for background emission and efficiency of six detectors for four centrality classes of the ^{36}Ar+^{58}Ni reaction at 50 MeV/nucleon. Data are represented by dots. The dashed lines is the multisource contribution of the QT, the dotted line is the contribution of the MRS and the full line is the sum of both. Statistical uncertainty is illustrated.

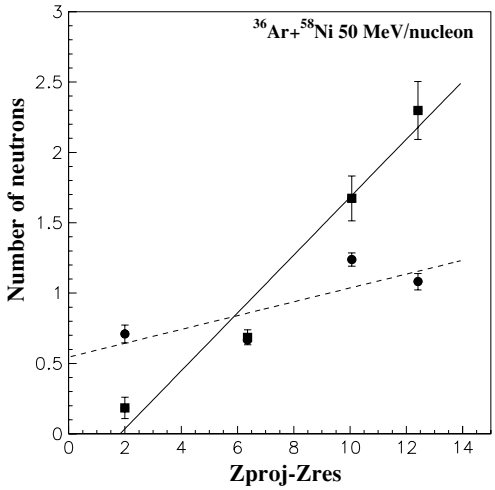

FIG. 7. Linearized neutrons multiplicities for ^{36}Ar+^{58}Ni at 50 MeV/nucleon as a function of the projectile charge minus the QP residue charge. QT (dots) and MRS (squares) multiplicities are illustrated. For each class of reaction, extracted multiplicities were placed at the statistical average of their Z_{res} interval.

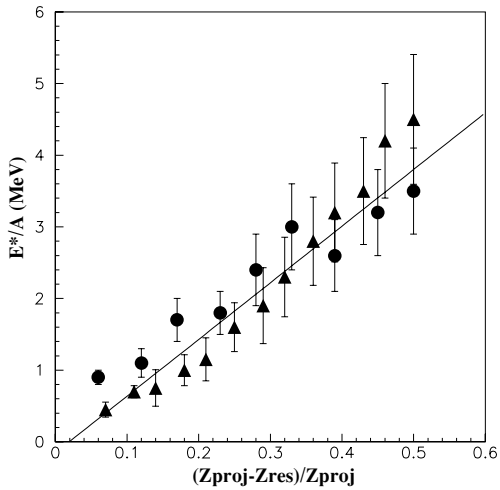

FIG. 8. Excitation energy per nucleon of the reconstructed QP as a function of the charge of projectile minus the charge of the QP residue over the charge of the projectile. Results for QP in ^{58}Ni+^{58}Ni at 52 MeV/nucleon (triangles) and for the QP in ^{40}Ar+^{27}Al at 40 MeV/nucleon [35] (dots) are shown. Linear fit for $Z_{proj} - Z_{res}/Z_{proj} \geqslant 0.1$ data is plotted.

the ^{58}Ni+^{58}Ni data showed that the fitting procedure applied to a backward subsample of the energy spectra can possibly result in some lowering of the midrapidity velocity obtained compared to that of the full distribution. That is caused by the increased numerical weight of the backward distributions in the fitting procedure. This effect, in the limits of the energy spectra uncertainty, could also explain to some extent the velocities obtained for the two most peripheral classes. The two most central classes of events do not seem to be affected by the angular asymmetry of the neutron energy distribution because the MRS velocities obtained are near the nucleon-nucleon velocity.

The deduced multiplicities for the MRS increase steadily with centrality and reach a value of 2.3, whereas QT multiplicities are stabilizing just above 1. Proton multiplicities are significantly higher for the ^{58}Ni QP than the neutron multiplicities for the ^{58}Ni QT. This enhancement of free protons can be partially understood if we assume a rather symmetric ($N/Z = 1.07$) nucleus that deexcites to reach the more neutron-rich evaporation attractor line [29] and thus emits more protons than neutrons. However, the observed quantitative difference cannot be fully explained by this scenario. For a coherent interpretation of the QP free nucleon multiplicities, other effects occuring in the dynamical deformation (neck) step of the collision should also contribute to this difference by lowering the N/Z ratio of the QP before its deexcitation begins (see Sect. V).

Neutron multiplicities deduced for the target and the MRS in the system ^{36}Ar+^{58}Ni are used to evaluate the neutron multiplicities for the QP and the MRS in the symmetric ^{58}Ni+^{58}Ni reaction. To compare the two experiments, the ^{58}Ni excitation energy is evaluated for each of the two systems and will be used as a link. It is assumed that if the ^{58}Ni QP in the ^{58}Ni+^{58}Ni reaction and the ^{58}Ni QT in the ^{36}Ar+^{58}Ni reaction have the same excitation energy per nucleon, they will emit the same number of free neutrons. Excitation energy evaluation is achieved with the relation

$$\left(\frac{E^*}{A}\right)_{QP} = C\left(\frac{Z_{proj} - Z_{res}}{Z_{proj}}\right) \tag{5}$$

where C is assumed to be the same constant for both ^{36}Ar and ^{58}Ni. This assumption was verified by evaluating Eq. (5) for the reconstructed QP excitation energy (calorimetry method) in the ^{58}Ni+^{58}Ni reaction and comparing it with calorimetry results for ^{40}Ar in Ref. [35]. Figure 8 illustrates this comparison.

Because HERACLES gives the charge of the ^{36}Ar projectile residue and not the charge of the ^{58}Ni target residue, two limiting assumptions were made to deduce the excitation energy of the ^{58}Ni QT, related to the charge of the target residue by Eq. (5): equal energy sharing (EES) and another one approching the equal temperature limit (ETL). For this last assumption, a mass ratio of 1.3 was used instead of the full mass ratio (1.6) of a EES case to deduce the excitation energy per nucleon of the ^{58}Ni QT. In the EES case, the total excitation energy available is split equally between the two partners regardless of their mass, in contrary to the "toward ETL" hypothesis in which a certain temperature equilibration (same E^*/A for both partners) is supposed. A temperature $1/T = \sqrt{a/E^*}$ is assumed, with a the level density parameter. Results of energy sharing experiments at intermediate energy show a clear tendency toward the EES hypothesis for a large range of centralities [38]. For each event analyzed in the ^{58}Ni+^{58}Ni reaction, the charge of the ^{58}Ni QP residue is taken as the charge of the ^{58}Ni QT residue in the ^{36}Ar+^{58}Ni reaction. Then a neutron multiplicity is selected according to the linearized relation of Fig. 7 and the EES hypothesis. Neutron multiplicities for the MRS have been added in the ^{58}Ni+^{58}Ni analysis according to the same excitation energy deduced for the QP. However, because those neutron multiplicities were extracted in the ^{36}Ar+^{58}Ni reaction, they should represent

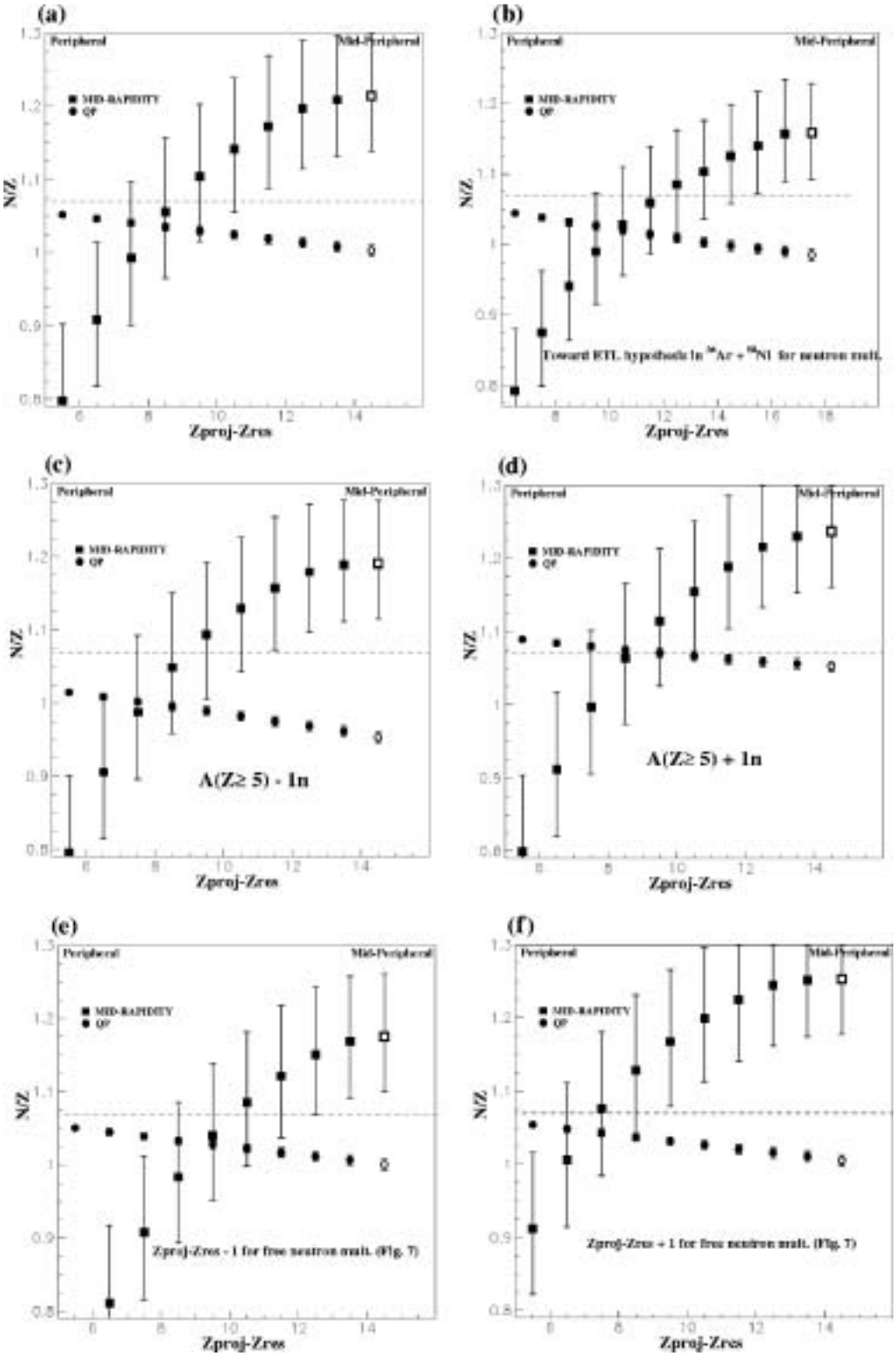

FIG. 9. (a) N/Z of QP and MRS for the reaction ^{58}Ni+^{58}Ni at 52 MeV/nucleon as a function of the charge difference between the projectile and the residue. (Solid squares) N/Z of MRS; (solid dots) N/Z of QP; (thin dotted line) original N/Z of the projectile and target (1.07). EES hypothesis in ^{36}Ar+^{58}Ni is assumed. (Open symbols) $Z_{\rm res}(^{36}{\rm Ar}) = 3.5$ rounded to 4. Errors due to multisource fit uncertainty for free nucleons are reported. (b) Same as (a) with the "toward ETL" hypothesis assumed in ^{36}Ar+^{58}Ni. (c) and (d) Same as (a) with one neutron removed or added to every $Z \geqslant 5$ fragment in the analysis. (e) and (f) Same as (a) with the $Z_{\rm proj} - Z_{\rm res}$ value decreased or increased by one unit for free neutrons selection in Fig. 7.

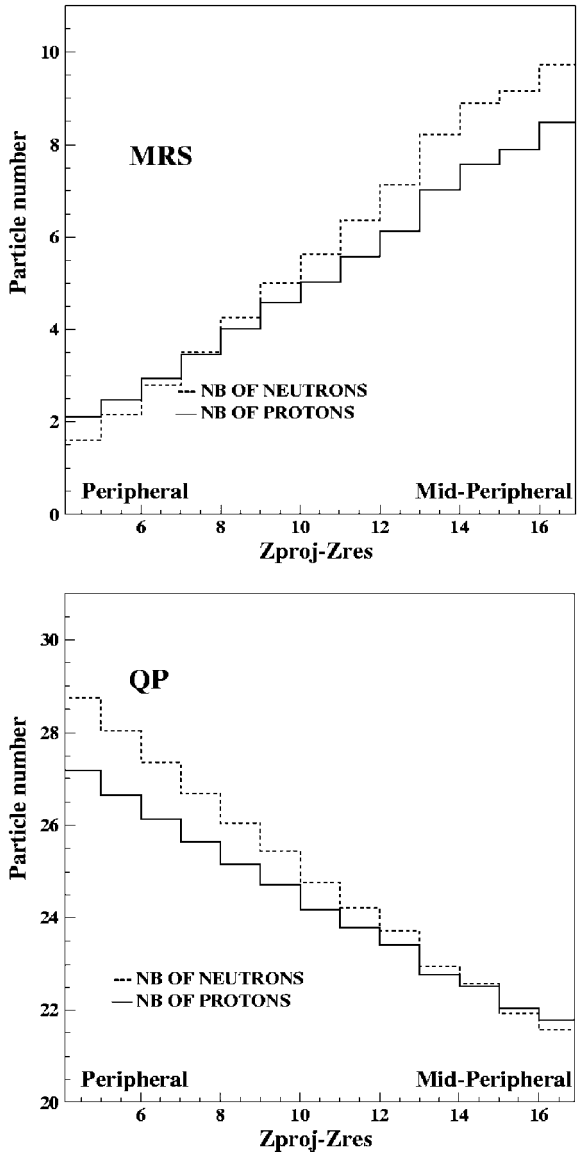

FIG. 10. Total number of neutrons (dashed lines) and protons (full lines) for MRS (upper panel) and QP (lower panel) as a function of the charge difference between the projectile and the residue. Graphs are for the reaction ^{58}Ni+^{58}Ni at 52 MeV/nucleon. EES hypothesis in ^{36}Ar+^{58}Ni is assumed.

a lower limit for the heavier and more neutron-rich system ^{58}Ni+^{58}Ni. This is discussed below.

IV. N/Z VALUES FOR MRS AND QP

A. Experimental N/Z evaluation

On an event-by-event basis, the ^{58}Ni QP and the MRS were reconstructed and free nucleon multiplicities were added according to the moving source parameter values for corresponding $Z_{\rm res}$(^{58}Ni). Linearized multiplicity relations of Fig. 5 and Fig. 7 are used to make the multiplicities continuous. N/Z composition for the total MRS and QP nuclear material (free nucleons, particles and all heavier fragments) as a function

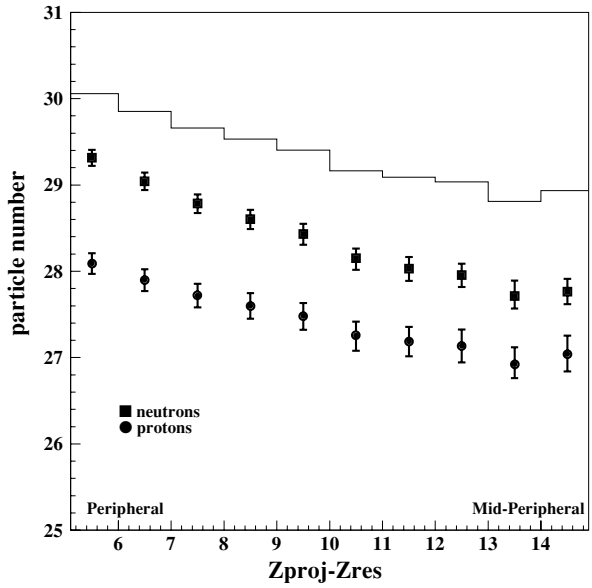

FIG. 11. Number of protons (dots) and neutrons (squares) of the reconstructed projectile in ^{58}Ni+^{58}Ni at 52 MeV/nucleon using 1/2MRS(Z, N)+QP(Z, N). (Solid line) Number of protons of the reconstruted projectile ($Z_{\rm reconstructed}$) multiplied by 1.07. EES hypothesis in ^{36}Ar+^{58}Ni is assumed. Errors due to multisource fit uncertainty for free nucleons are reported.

of $Z_{\rm proj} - Z_{\rm res}$ is presented in Fig. 9. Figure 10 shows average total number of protons and neutrons present in QP and MRS as a function of $Z_{\rm proj} - Z_{\rm res}$. Figure 9 shows the average value of N/Z ratios computed at each event, this is not to be confused with the ratio of the average number of neutrons over the average number of protons in Fig. 10.

The general trend is that the N/Z ratio of the QP decreases sligthly with the centrality of the collision, whereas the N/Z of the MRS increases for more central collisions to reach a higher N/Z value than that of the QP and that of the original system (1.07). On average, the QP (and presumably the QT) seems to transfer a small number of neutrons to the MRS, that does not affect much its numerical N/Z value due to its larger size. However, this small amount of neutrons does enhance the neutron richness of the MRS due to its smaller size. Figure 3 shows that the charge in the QP can be around 3 times the charge in the MRS for the most central events studied here (when $Z_{\rm res}$ is added). According to the QP and MRS N/Z ratios in Fig. 9, that neutron transfer is seen to increase with centrality, meaning that it could depend on the contact time of the two nuclei and on the deformation between them. For the most central collisions in panel (a) of Fig. 9, MRS N/Z ratios reach values of 1.2. Meanwhile, the QP N/Z drops at values close to 1. As stated before, hypotheses regarding the mass of $Z \geqslant 5$ fragments do not affect significantly the MRS N/Z ratio [see panels (c) and (d) of Fig. 9]. Those panels show that for the QP N/Z ratio, results obtained with one neutron added or removed to every $Z \geqslant 5$ fragments would have a range of about ± 0.04 on the N/Z ratio values. A similar test has been done by varying the charge of the ^{36}Ar residue by ± 1 charge unit in the selection of the number of free neutrons from Fig. 7 [see panels (e) and (f) of Fig. 9]. The QP N/Z ratio

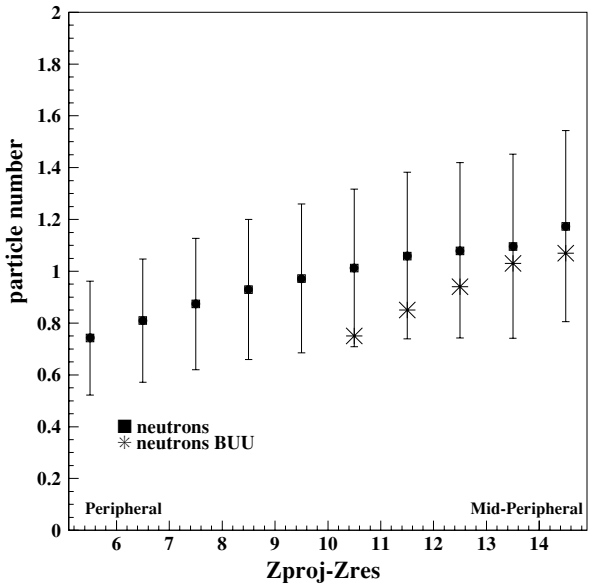

FIG. 12. Number of neutrons missing in Fig. 11 to recover $1.07^{*}Z_{\text{reconstructed}}$. EES hypothesis in ^{36}Ar+^{58}Ni is assumed. Errors due to multisource fit uncertainty for free nucleons are reported. Stars show prediction of BUU simulations regarding MRS free neutrons multiplicities difference between ^{58}Ni+^{58}Ni at 52 MeV/nucleon and ^{36}Ar+^{58}Ni at 50 MeV/nucleon.

is not affected significantly and the MRS N/Z ratio changes by about ± 0.04 for $Z_{\text{proj}} - Z_{\text{res}} \geqslant 10$ (most central collisions). Those tests show that the results are quite stable to changes in mass hypothesis or excitation energy errors. For the most peripheral collisions in Fig. 9, MRS N/Z ratio is low and below 1. Pollution of N/Z symmetric particles coming from the target (see Fig. 3) could contribute to this result. In an equal-mass reaction such as ^{58}Ni+^{58}Ni, symmetry can be assumed in the dynamical deformation between target and projectile [16] so that QP and QT should, on average, have an equal contribution to the population of the MRS. This leads to believe that the N/Z results in Fig. 9 for the most peripheral reactions are nonphysical. Indeed, the fact that both MRS and QP present a N/Z ratio below 1.07 simultaneously is impossible if the measurement of the QP and MRS is complete. The addition of the nuclear material attributed to the QP and half of the material attributed to the MRS should give, on average, a value of $Z = 28$ and $N = 30$, which is the reference point of the original projectile. Still using the neutron multiplicities extracted from the reaction ^{36}Ar+^{58}Ni, it is instructive to plot the number of neutrons and protons obtained in this manner as a function of centrality. Figure 11 shows that the number of protons in the reconstructed projectile goes from an average value of about 28.1 (peripheral) to an average value of 27.2 (more central). The fact that this value is not exactly equal to 28 can be explained by the uncertainty on the proton multisource analysis, the velocity selection of the MRS, detection efficiency and experimental thresholds. Except for the multisource fit uncertainty for free protons, other sources of errors, for the rather N/Z symmetric ^{58}Ni+^{58}Ni system, should remove or add approximatively the same number of protons and neutrons according to the initial system N/Z because those nucleons are in bound matter. So, after accounting for selection and experimental bias, the N/Z of the reconstructed projectile for a charge higher than 27 should be around its original value, 1.07, even if some clusterized material is missing. From Fig. 11 we clearly see that there are some neutrons missing to get the original N/Z value of 1.07. Figure 12 shows the number of missing neutrons, as a function of centrality, to recover the initial projectile N/Z of 1.07. Putting aside the uncertainty on the mass of $Z \geqslant 5$ frements, the missing free neutrons needed to recover the initial N/Z ratio of 1.07 could mainly come from the mass difference between the ^{36}Ar+^{58}Ni reaction and the ^{58}Ni+^{58}Ni reaction. In particular, the structure difference between the lighter perfectly symmetrical ^{36}Ar projectile and the heavier slightly asymmetrical ^{58}Ni projectile could influence the number of free neutrons produced in the midrapidity region during the phase of contact between the target and projectile.

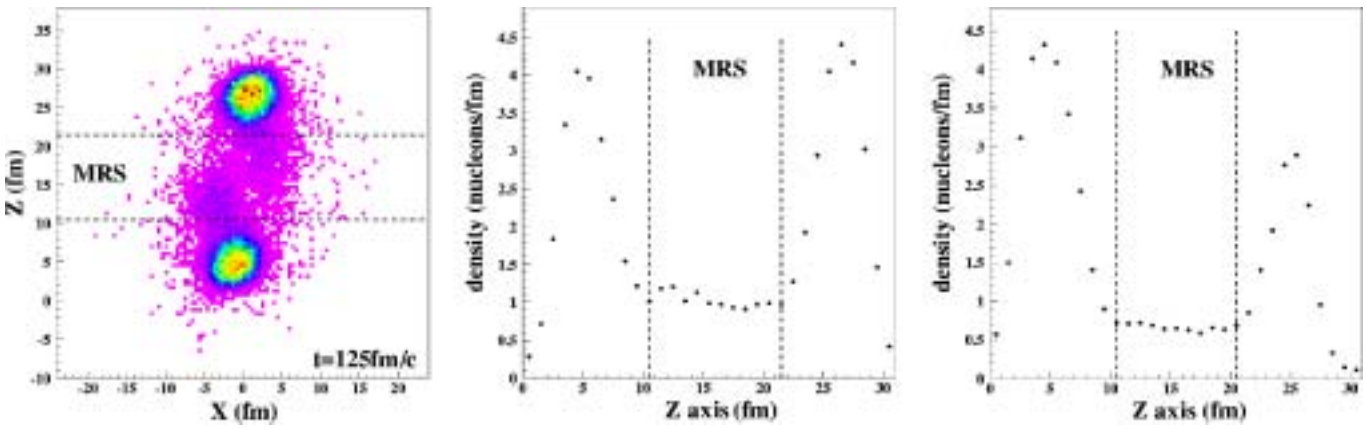

FIG. 13. (Color online) (Left) Bidimensionnal density profile at 125 fm/c for a simulated ^{58}Ni+^{58}Ni reaction at 52 MeV/nucleon with an impact parameter of 4 fm. (Center) Projection of the density profile on the z axis (projectile direction) for the same reaction as in the left panel at 125 fm/c. (Right) Projection of the density profile on the z axis (projectile direction) at 125 fm/c for a simulated ^{36}Ar+^{58}Ni reaction at 50 MeV/nucleon with an impact parameter of 3.7 fm. Midrapidity limits are surimposed on the three graphics.

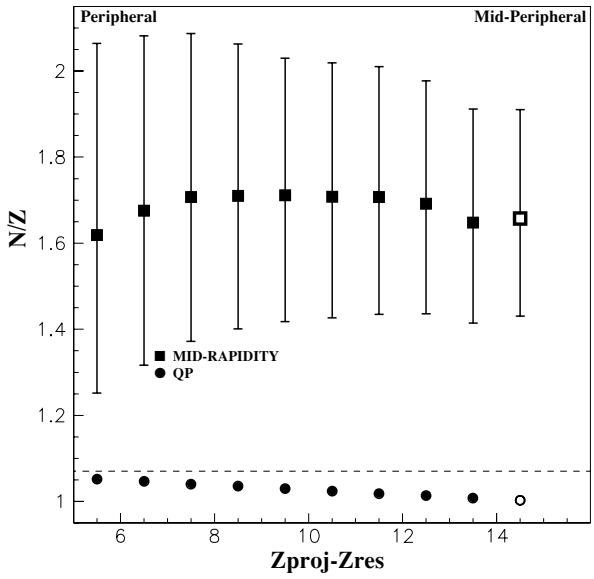

FIG. 14. N/Z of QP and MRS for the reaction ^{58}Ni+^{58}Ni at 52 MeV/nucleon as a function of the charge difference between the projectile and the residue. Neutrons missing to recover $N/Z = 1.07$ in reconstructed projectile are added in MRS. (Solid squares) N/Z of MRS; (Solid dots) N/Z of QP; (thin dotted line) original N/Z of the projectile and target (1.07). EES hypothesis in ^{36}Ar+^{58}Ni is assumed. (Open symbols) $Z_{\rm res}(^{36}{\rm Ar}) = 3.5$ rounded to 4. Error due to multisource fit uncertainty for free nucleons is reported.

B. BUU simulations

To investigate if the number of missing neutrons in the reconstructed ^{58}Ni projectile is compatible with the above hypothesis that missing neutrons come from differences in MRS, BUU simulations [39] were done for both reactions: ^{58}Ni+^{58}Ni at 52 MeV/nucleon and ^{36}Ar+^{58}Ni at 50 MeV/nucleon. In those simulations, the BUU transport equation is solved using a test-particle approach. A Skyrme interaction combined with a density independent symmetry term is used. The mean-field nuclear potential is of the following form:

$$U_{n,p}(\rho) = \alpha\left(\frac{\rho}{\rho_0}\right) + \beta\left(\frac{\rho}{\rho_0}\right)^{\sigma} - 2C\frac{(\rho_n - \rho_p)}{\rho_0}\tau_z, \qquad (6)$$

where C is the constant related to the symmetry energy, ρ the total density ($\rho_p + \rho_n$), and τ_z the isospin of the nucleon (+1/2 for proton and $-1/2$ for neutron). C was adjusted to 20 MeV by using the ground state energies of nuclei. The constants α and β related to the compressibility were fixed to -356 and 303 MeV, respectively, which is the parametrization for a soft equation of state ($K = 210$ MeV). Coulomb interaction is also included. In-medium nucleon-nucleon collision cross sections [40,41] were used and Pauli blocking evaluated. Guided by the spatial density profiles projected on the Z axis (beam direction), midrapidity limits were fixed at 125 fm/c, corresponding to the limit of MRS in velocity space. Nuclear material in those limits was studied. Figure 13 shows a bidimensional density profile representation of the ^{58}Ni+^{58}Ni reaction at 52 MeV/nucleon and the midrapidity limits surimposed on it; projections on the Z axis are also shown for both reactions. Free MRS neutron multiplicities obtained in the ^{36}Ar+^{58}Ni reaction (Fig. 7) were multiplied by the ratio of total neutrons produced in the simulated ^{58}Ni+^{58}Ni MRS over those produced in the simulated ^{36}Ar+^{58}Ni MRS. This procedure assumes that the ratios of free neutrons over total neutrons in the MRS is about the same in the two reactions. This assumption restricts the validity of the simulations to the most central collisions studied here. Sufficient material must be emitted from the MRS to avoid the effects of a small number of nucleons in the MRS that would make the above hypothesis rather fragile. Consequently, results of midperipheral BUU calculations will be compared with experimental data for which $Z_{\rm proj} - Z_{\rm res} \geqslant 10$. The ratio of total neutrons found in MRS of the two reactions, averaged over impact parameters from 3 to 4.5 fm, was found to be 1.86 (compared to 1.25 for the ratio of neutron number in both systems). Reactions with impact parameters from 3 to 4.5 fm for the simulated ^{58}Ni+^{58}Ni reaction present an average number of proton in the MRS equal to 9.63. The experimental centrality class $Z_{\rm proj} - Z_{\rm res} =$ 16 (14) has an average number of 8.9 (8.0) MRS total proton. Considering the uncompleteness of the system (and MRS) reconstruction (Fig. 11), the BUU simulations should be valid for the most central collisions studied here. The MRS free neutron differences predicted by BUU are then reproduced in Fig. 12, for $Z_{\rm proj} - Z_{\rm res} \geqslant 10$, where the missing neutrons in the ^{58}Ni projectile reconstruction are shown. The agreement between the missing neutrons and the experimental results is good in the most central collisions.

C. N/Z evaluation with free neutron correction

Figure 14 is the same as panel (a) of Fig. 9 with free neutrons added to the MRS to compensate as realistically as possible for the difference in the MRS formation between the ^{58}Ni+^{58}Ni reaction and the ^{36}Ar+^{58}Ni reaction. Values of Fig. 12 were taken after being checked in the previous subsection by BUU simulations. For Fig. 14, large error bars, due to uncertainty from the moving source analysis on original and added free nucleons, prohibit any precise estimation of the evolution of the MRS N/Z as a function of centrality. The N/Z of the MRS nuclear material is around 1.65 with approximate limits of 1.4–2.0. The nonphysical region present in Fig. 9 (see Sec. IV A) before the adjustment of MRS free neutron multiplicity is nonexistent and the results are mathematically plausible.

V. DISCUSSION

First, Fig. 3 shows that the clusterized $A \geqslant 2$ particles in the MRS present a clear neutron excess and that QP emitted particles are symmetric regarding their neutron and proton content over the whole centrality range. Second, free nucleons were included. Free proton multiplicities are extracted directly from the ^{58}Ni+^{58}Ni reaction, and free neutron multiplicities, extracted from ^{36}Ar+^{58}Ni at 50 MeV/nucleon, are added to the ^{58}Ni+^{58}Ni reaction using excitation energy as a link. We can reasonably consider the MRS free neutron multiplicity obtained from a lighter and more symmetric system as a lower

limit for the ^{58}Ni+^{58}Ni reaction. QT neutron multiplicities extracted in the HERACLES experiment should be a correct approximation of those from the QP in the INDRA experiment. Even with free neutron multiplicities coming from a lighter system, a significant increase in the MRS N/Z ratio is already seen. In the last step of the analysis, an attempt to evaluate the MRS free neutron differences between the two reactions studied is made by comparing the projectile reconstruction and BUU simulations. The nonphysical region of neutron deficiency present in the first graphic (Fig. 9) disappears with this procedure but a large uncertainty is introduced in the MRS N/Z evaluation. Despite this fact, the MRS N/Z ratio is seen above 1.07 and, coherent with this observation, the QP N/Z is below that of the original system (1.07).

A possible schematic explanation to the results obtained here is that the projectile and target lose nuclear material in the midrapidity region during the time of contact between them and a net flow of neutrons in the MRS occurs during this phase of the reaction leaving the QP and QT neutron-poor in comparaison to their initial N/Z value. This fact would explain the low number of free neutrons, compared to free protons, emitted subsequently by the QP to reach the attractor line.

Interestingly, simulations for the ^{112,124}Sn+^{112,124}Sn systems [42] using the transport equation of Boltzmann-Nordheim-Vlasov (BNV) with a density-dependent symmetry energy reproduce the main tendencies observed here. An increase of the N/Z asymmetry is obtained in the MRS region due to proton-neutron density migration among the MRS, QP, and QT regions [42].

Neutron-rich IMFs favorably emitted by a rotating QP source and Coulomb pushed toward midrapidity is an interesting statistical explanation proposed [22] for the neutron enrichment of the MRS IMFs. It would be instructive to verify this scenario quantitatively for a middle size system such as ^{58}Ni+^{58}Ni because it was originally elaborated using a SMM simulation of a Au+Au reaction. The abundance of free neutrons in the MRS is a subject that would also have to be addressed in this model.

Differences in the present results here and those shown in [21] could be due to the differences in system size, system N/Z asymmetry, source reconstruction procedures, mass hypotheses, and different centrality ranges covered in the analysis.

VI. CONCLUSION

In summary, we observed that the N/Z ratio of QP decreases and that of MRS increases with respect to the centrality of the collision in the reaction ^{58}Ni+^{58}Ni at 52 MeV/nucleon. Despite the lack of direct measurement for the MRS free neutron multiplicities, limiting assumptions lead to N/Z ratios behaviors that suggest the existence of an asymmetric migration of neutrons and protons between QP and MRS, what would make the MRS enriched in neutron compared to the original system N/Z ratio (1.07). This was done by applying a statistical QP reconstruction procedure, using isotopically resolved fragments up to $Z = 4$ in the INDRA multidetector, assumptions on the mass of the heavier fragments using evaporation model [29] and an estimate of free nucleon multiplicities deduced via a moving source analysis in the reactions ^{58}Ni+^{58}Ni at 52 MeV/nucleon and ^{36}Ar+^{58}Ni at 50 MeV/nucleon. The MRS N/Z ratio is seen at values higher than that of the initial system (1.07) and higher than that of the QP that decreases slightly to a value less than the one of the initial system. Further theoretical and experimental work will be needed to better understand the neutron and proton content of the midrapidty region and to settle the question of MRS neutron enrichment for systems of various sizes and N/Z asymmetries. Especially, an experiment that would allow a simultaneous measurement of charged particles and free neutrons in the same setup, would improve the precision of N/Z ratio results.

ACKNOWLEDGMENTS

The authors thank Wolfgang Bauer for the use of his BUU code. This work was supported in part by the Natural Sciences and Engineering Research Council of Canada, the Fonds pour la Formation de Chercheurs et l'Aide à la Recherche du Québec, the Robert A. Welch Foundation through Grant No. A-1266, and the Department of Energy through Grant No. DE-FG03-93ER40773.

[1] J. Tõke *et al*., Phys. Rev. Lett. **75**, 2920 (1995).
[2] J. Lukasik *et al*. [INDRA Collaboration], Phys. Rev. C **55**, 1906 (1997).
[3] C. P. Montoya *et al*., Phys. Rev. Lett. **73**, 3070 (1994).
[4] J. F. Lecolley *et al*., Phys. Lett. **B354**, 202 (1995).
[5] Y. Larochelle *et al*., Phys. Rev. C **55**, 1869 (1997).
[6] T. Lefort *et al*., Nucl. Phys. **A662**, 397 (2000).
[7] L. Gingras *et al*., Phys. Rev. C **65**, 061604 (2002).
[8] S. Piantelli *et al*., Phys. Rev. Lett. **88**, 052701 (2002).
[9] Z. He *et al*., Phys. Rev. C **63**, 011601 (2001).
[10] Z. He *et al*., Phys. Rev. C **65**, 014606 (2002).
[11] H. Xu *et al*., Phys. Rev. C **65**, 061602 (2002).
[12] G. Poggi., Nucl. Phys. **A685**, 296 (2001).
[13] D. Doré., Phys. Lett. **B491**, 15 (2000).
[14] J. Colin *et al*., Phys. Rev. C **67**, 064603 (2003).
[15] Ph. Eudes *et al*., Phys. Rev. C **56**, 2003 (1997).
[16] A. Chernomoretz *et al*., Phys. Rev. C **65**, 054613 (2002).
[17] Y. Larochelle *et al*., Phys. Rev. C **62**, 051 602(R) (2000).
[18] J. F. Dempsey *et al*., Phys. Rev. C **54**, 1710 (1996).
[19] E. Plagnol *et al*., Phys. Rev. C **61**, 014 606 (2000).
[20] P. M. Milazzo *et al*., Phys. Lett. **B509**, 204 (2001).
[21] L. G. Sobotka *et al*., Phys. Rev. C **62**, 031 603(R) (2000).
[22] A. S. Botvina and I. N. Mishustin., Phys. Rev. C **63**, 061601 (2001).
[23] H. Müller and B. D. Serot., Phys. Rev. C **52**, 2072 (1995).
[24] M. Colonna *et al*., Phys. Rev. C **57**, 1410 (1998).
[25] M. di Toro *et al*., Nucl. Phys. **A681**, 426c (2001).
[26] V. Baran *et al*., Nucl. Phys. **A632** , 287 (1998).

[27] J. Pouthas *et al*., Nucl. Inst. and Meth. A **357**, 418 (1995).
[28] N. Nakao *et al*., Nucl. Instr. Meth. Phys. Res. A **362**, 454 (1995).
[29] R. J. Charity., Phys. Rev. C **58**, 1073 (1998).
[30] L. Gingras *et al*., XXXVI International Winter Meeting on Nuclear Physics, Bormio (Italy), 265 (1998).
[31] R. J. Charity *et al*., Nucl. Phys. **A483**, 371 (1988).
[32] L. Tassan-Got and C. Stéphan, Nucl. Phys. **A524**, 121 (1991).
[33] R. Wada *et al*. Phys. Rev. C **39**, 497 (1989).
[34] Y. Larochelle *et al*., Phys. Rev. C **59**, 565 (1999).
[35] G. Lanzano *et al*., Nucl. Phys. **A683**, 566 (2001).
[36] T. Ericson, Adv. Phys. **9**, 425 (1960).
[37] A. S. Goldhaber, Phys. Rev. C **17**, 2243 (1978).
[38] G. Casini *et al*., Eur. Phys. J. A **9**, 491 (2000).
[39] W. Bauer *et al*., Phys. Rev. C **34**, 2127 (1986).
[40] G. Q. Li and R. Machleidt., Phys. Rev. C **48**, 1702 (1993).
[41] G. Q. Li and R. Machleidt., Phys. Rev. C **49**, 566 (1994).
[42] V. Baran *et al*., Nucl. Phys. **A703**, 603 (2002).